Universiteit Utrecht

Opleiding Natuur- en Sterrenkunde

Inverse design of interactions for single particle quasicrystals

Bachelor Thesis

Maurice Dijsselbloem

Supervisors:

Dr. Marjolein Dijkstra
Debye Institute

June 12, 2019

Abstract

In this thesis, we will attempt to inverse design the interactions for single particle quasicrystals. We use 2D Monte Carlo simulations with a square shoulder potential of width 1.4σ. We calculate the pair correlation function $g(r)$ for various densities and temperatures. A quasicrystal is expected to form at a crossover line at which the pair correlation function transforms from one form to the other. We attempt to find a crossover line with two different methods. One of these methods resulted in a crossover line, but no quasicrystals have been found yet around this line.

Contents

1 Introduction

In this thesis, we will attempt to inverse design a quasicrystal using single particle Monte Carlo simulations. We search for a crossover line where the form of the pair correlation function $g(r)$ changes from one form to another. To find a crossover line we use two different methods. Firstly, we use the Ornstein-Zernike equation and performing a pole analysis. Secondly, we manually look at the first two peaks of the pair correlation function and look for points in the (T, ρ) plane where the first peak becomes bigger than the second one.

A quasicrystal is a solid that seems to have some form of order, but it doesn't have translational symmetry like real crystals have. For example, normal crystals can be brought back to a single unit cell that is repeated in every direction. Quasicrystals on the contrary, can't be brought back to a unit cell, while they do fill all space. Their tiling is completely random and never repeats [1]. Another interesting property of quasicrystals is that they have a rotational symmetry that normally is not allowed. Normal crystals can have 2, 3, 4 or 6 fold rotational symmetries, but quasicrystals have other rotational symmetries. For example, a 2D quasicrystal can have a 12 fold (dodecagonal) rotational symmetry [2]. Quasicrystals have been found several alloys and in soft-matter systems. The first one was discovered experimentally in 1984 [3]. Most known quasicrystals today are synthesised and consist of multiple particles. There is a known quasicrystal that appears in nature [4].

Quasicrystals are thought to arise due to two competing length scales. These different length scales can, for example, be created with different sized particles. [5] A different way, and the one that is used in this thesis, is to use a single particle system, but choose a potential that can give rise to two different length scales. Monte Carlo simulations confirm that quasicrystals can arise with both methods [6, 7].

Important research has been done by Dotera *et al* where various single particle quasicrystals with 10, 12, 18 and 24 fold symmetries have been found using Monte Carlo simulations with a hard-core square shoulder potential [2]. In this paper we also choose to use this hard-core square shoulder potential. This potential is more thoroughly explained in the theory section.

It is interesting to investigate the formation of quasicrystals in simulations, because it might help us understand the circumstances where quasicrystals form. Understanding where and how the quasicrystals form, might help with synthesising these crystals experimentally.

2 Theory and methods

2.1 Potential

Our simulation is a two-dimensional system with hard disks particles with diameter σ. We want these particles to adhere to certain rules. For example, we don't want two particles to be in the same point of space. To make the particles interact, we need to choose a potential. A potential describes the energy of a particle that is a certain distance from another particle. The hard-core square shoulder potential has a hard-core with a soft area around the core [8]. This means that the potential is infinite for distances r smaller than the particle diameter σ, and the potential is a fixed ϵ for distances between $r = \sigma$ and $r = \delta\sigma$, where δ is called the shoulder of the potential. It is zero for distances $r > \delta\sigma$. Since ϵ is positive, the potential

works repulsive at short distances. Together the hard-core square shoulder potential reads

$$V(r) = \begin{cases} \infty, & r < \sigma \\ \epsilon, & \sigma < r < \delta\sigma \\ 0. & r > \delta\sigma \end{cases} \tag{1}$$

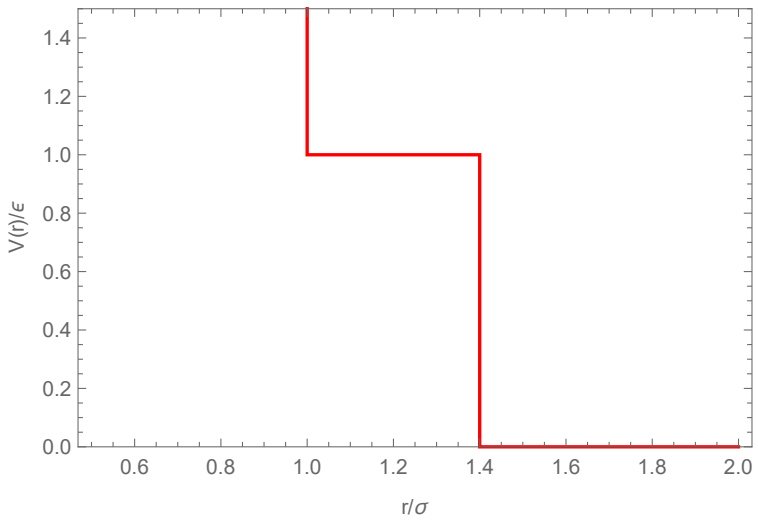

Figure 1: Representation of the hard-core square shoulder potential. The potential is infinite for r smaller than the particle diameter σ. It has a value of ϵ for values bigger than σ, but smaller than the shoulder width $\delta\sigma$. In this case $\delta = 1.4$

For most simulations done in this paper, we use a shoulder δ of 1.4 and a value for ϵ of 1 (see figure 1). This shoulder is chosen such that it is approximately the square root of 2. This means it favours both triangular and square length scales. In earlier research, it has been shown that this should result in a dodecagonal quasicrystal [2, 9, 10].

A physical system this shoulder can represent is a particle with an (hard) aromatic core and (soft) alkyl chains [9]. The aromatic core represents the part in the potential that is infinite, while the alkyl chains are deformable and thus represent the part where it is ϵ. Another system at which the potential has been used is the interactions of Cesium or Cerium atoms [11].

2.2 Monte Carlo simulation

We need a way of simulating Crystals and their stability. To do this, we use Monte-Carlo simulations. In the following subsections we largely follow the discussion from reference [12].

In a Monte Carlo move we randomly choose a particle in the box. This particle is moved a random amount between $-\Delta$ and Δ in both x and y directions. The energy of the particle is calculated before and after a move. If the new energy of the system is lower than the old energy, the move is always accepted. If the energy is higher, the chance of move acceptance is calculated by the Boltzmann weight

$$W = e^{-\frac{dE}{k_B T}}. \tag{2}$$

Here dE is the energy difference, k_B is the Boltzmann constant and T the temperature. The chance of move acceptance with the hard-core square shoulder potential would thus be

$$P(acc) = \begin{cases} 0, & r < \sigma \\ e^{-\frac{\epsilon}{k_B T}} = e^{-\frac{1}{T^*}}, & r > \sigma \\ 1, & r > \sigma \end{cases} \tag{3}$$

where $T^* = \frac{k_B T}{\epsilon}$ is the reduced temperature. If Δ is too low, it would mean our simulation is not very efficient, because the particles would barely move and almost every move would be accepted. If we choose a value for Δ that is too high, the chance of overlapping particles would be very large and almost every move would be rejected. To make the simulation most efficient, the value for Δ should be chosen such that the chance of accepting a move is around 50%. In one Monte Carlo cycle we attempt to move the same number of particles, as there are in the box.

2.2.1 Canonical ensemble

The Monte Carlo simulations are performed in the canonical (N, V, T) ensemble. Where N is the number of particles, V the volume and T the temperature of the system. These are held constant throughout the simulation. This also means that the density ρ can be held constant. In simulations it is convenient to use the reduced density $\rho^* = \frac{N\sigma^2}{V}$ and the reduced temperature $T^* = \frac{k_B T}{\epsilon}$. This will make certain that the results will always be the same for the same T^* and ρ^*.

2.2.2 Periodic boundary conditions

We don't want a surface in the box to interact with the particles. Our number of particles is relatively small. Creating a hard border at the edge of the box could potentially have a big influence in how the particles behave. To make the box bigger than it actually is, we can use Periodic Boundary Conditions (PBC). When periodic boundary conditions are implemented, the box has no walls. When a particle reaches the edge of the box, it disappears and reappears at the other end of the box.

Because of the periodic boundary conditions, there are multiple ways we can draw a straight line between two particles. This causes trouble when we want to calculate the distance between these particles, because we only want the shortest distance to calculate the energy. To fix this problem, we use the nearest image convention. If the particle distance is bigger than half the box size, we add or subtract a full box length to the distance. This makes sure we always have the shortest distance between two particles.

2.2.3 Cell lists

The simulations contain a lot of particles and the potential has a finite length. This means that the energy between a lot of particles is zero. A lot of time is wasted on calculating the energy between these particles. To speed up calculations we've implemented cell lists to the simulation. This method divides the box up to different cells. Of each cell it is known which particles it contains. This way the energy difference can be calculated by only summing over

the particles in the current cell of a particle and the neighbouring cells. This method can speed up the simulations significantly and we measured an increase in simulation speed of up to 30 times, which meant that we were able to do a lot more Monte Carlo steps than before. However, it is important that grid cells are chosen big enough, so that they are still bigger than the particles.

2.2.4 Equilibation

To see if a simulation is finished, we can look of the total energy of the system. If it hasn't changed much in the last moves, we can assume that the energy is stable and thus the simulation has reached an equilibrium state. After the system has reached an equilibrium state, we can start measuring the relevant parameters.

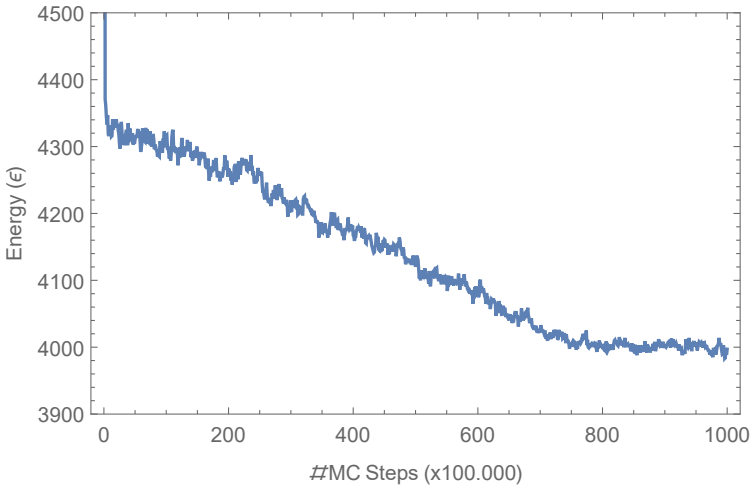

Figure 2: Plot of the energy as a function of Monte Carlo cycles. The used parameters were $T^* = 0.25, \rho^* = 0.945, \delta = 1.4$ and $N = 1840$. In the figure it visible that the energy goes down at first, but eventually the simulation reaches an equilibrium and doesn't change much anymore. In this case it seems the system equilibrates after 80 million Monte Carlo cycles.

2.2.5 Starting configuration

As a starting configuration, we choose a hexagonal lattice as in figure 3. Most simulations done in this work are 100 million Monte-Carlo cycles long, have a number of particles $N = 1840$ and have a shoulder $\delta = 1.4$.

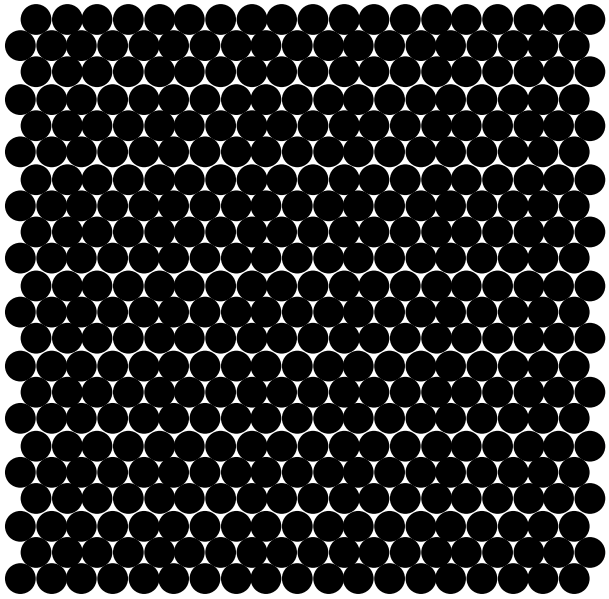

Figure 3: A hexagonal lattice is used as a starting configuration. In this case $N = 418$ which is less than most simulations performed.

2.3 Pair correlation function $g(r)$

To get insight of how particle distances are correlated, we can construct a pair correlation function $g(r)$. This function is essentially the occurrence of particle distances divided by a weight factor. For large r, when there is no more correlation, it goes to 1. It is calculated as

$$g(r) = \frac{V}{N^2}\left\langle \sum_{i=1}^{N}\sum_{j\neq i}^{N} \delta(\mathbf{r} - \mathbf{r}_{ij}) \right\rangle, \tag{4}$$

where δ is the Dirac delta function, and $\mathbf{r}_{ij} = \mathbf{r}_i - \mathbf{r}_j$ is the distance vector between the particles i and j. The way it is calculated in my simulation is by creating a histogram of particle distances and dividing them by n_{id}. In formula form this reads

$$g(r + 0.5\delta r) = \frac{1}{N}\frac{n_{his}(b)}{n_{id}(b)}, \tag{5}$$

where b is the bin and n_{id} is (for a 2D system)

$$n_{id} = \pi\rho[(r + dr)^2 - r^2]. \tag{6}$$

Because the system is not always in a perfect state, the pair correlation functions are calculated from the last ten snapshots of a simulation. The final pair correlation function is an average of these ten functions. This helps factoring out any randomness that might appear in a single snapshot. An examples of pair correlation functions are shown in figure 4.

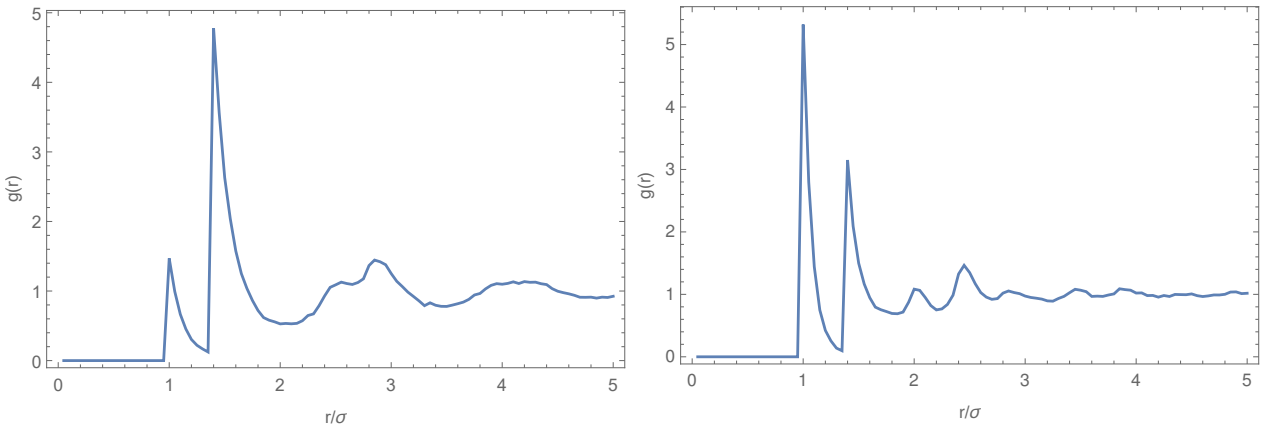

(a) (b)

Figure 4: The pair correlation function $g(r)$ for a simulation with parameters $T^* = 0.25$ and $\delta = 1.4$ after 100 million Monte Carlo cycles. For figure (a) the density is $\rho^* = 0.5$ and for figure (b) the density is $\rho^* = 0.7$. The pair correlation is calculated from the last 10 snapshots of the simulation and averaged.

As we see in figure 4, the pair correlation function has a peak at $r = \sigma$ and $r = \delta\sigma$. After those we see multiple smaller peaks. As the density of the simulation increases, the first peak at $r = \sigma$ will increase and the second at $r = \delta\sigma$ will decrease.

2.4 Ornstein-Zernike

The total correlation function $h(r_{12})$ is defined as

$$h(r_{12}) = g(r_{12}) - 1. \tag{7}$$

The Ornstein-Zernike equation splits the influence of the total correlation function $h(r_{12})$ in two parts. It can be written as

$$h(r_{12}) = c(r_{12}) + \rho \int c(r_{13})h(r_{32})d\mathbf{r}, \tag{8}$$

where $c(r)$ is an unknown function called the direct correlation function. The Ornstein-Zernike equation splits the influence in a direct part $c(r_{12})$, that describes the influence of particle 1 on particle 2, and an indirect part, that describes the influence of particle 1 on another particle 3. This particle 3 also influences particle 2 directly and indirectly. Usually the Ornstein-Zernike equation is solved with an extra relation between $h(r)$ and $c(r)$, called a closure. However, in our simulation we have a way of calculating the total correlation function $h(r)$ directly and use this to calculate the direct correlation function $c(r)$. To solve this, we can write this Ornstein-Zernike equation in terms of the Fourier transforms

$$\hat{h}(q) = \hat{c}(q) + \rho\hat{c}(q)\hat{h}(q). \tag{9}$$

We can rewrite this equation to find $\hat{c}(q)$ or $\hat{h}(q)$:

$$\hat{c}(q) = \frac{\hat{h}(q)}{1 + \rho\hat{h}(q)}, \tag{10}$$

$$\hat{h}(q) = \frac{\hat{c}(q)}{1 - \rho\hat{c}(q)}. \tag{11}$$

With $q = \alpha_1 + i\alpha_0$. Where the 2D Fourier $\hat{f}(k)$ transform of a function $f(r)$ is [13]

$$\hat{f}(q) = 2\pi \int_0^\infty J_0(rk) f(r) r dr. \tag{12}$$

The inverse Fourier transform is given by

$$f(r) = \frac{1}{2\pi} \int_0^\infty J_0(rq) \hat{f}(q) q dq, \tag{13}$$

with J_0 the zeroth order Bessel function.

The decay of $h(r)$ is determined by the poles $q = \alpha_1 + i\alpha_0$ that satisfy the relation [14][13]

$$1 - \rho\hat{c}(q) = 0. \tag{14}$$

Every $h(r)$ can be described by one of two different forms [13]. If $q = i\tilde{\alpha_0}$ is purely imaginary the solution is of the form

$$h(r) \approx \tilde{A} \frac{-e^{\tilde{\alpha_0} r}}{\sqrt{r}}, \tag{15}$$

with $\tilde{A}$ the amplitude. If the real part is non-zero $q = \alpha_1 + i\alpha_0$, $h(r)$ is of the form

$$h(r) \approx \frac{A e^{-\alpha_0 r} cos(\alpha_1 r + \theta)}{\sqrt{r}}, \tag{16}$$

with A the amplitude and θ a phase. The total correlation function changes from one form to the other as the density of the simulation increases. At this so-called crossover it is expected that a quasicrystal can form.

2.5 Crossover in the pair correlation function $g(r)$

A different way of approaching a crossover is looking directly at the peaks of the pair correlation function $g(r)$. As earlier mentioned, this function has peaks at $r = \sigma$ or at $r = \delta\sigma$. Here we will focus mostly on those first two peaks. As the density of the simulation is increased, the peak of $r = \delta\sigma$ will become smaller, and the peak at $r = \sigma$ becomes bigger. The density at which both peaks are of equal height, could be a region at which quasicrystals might form. We can investigate where these two peaks are of equal height for various temperatures.

2.6 Diffraction pattern

Since it is hard to determine if a quasicrystal has formed by just looking at the lattice, we need a method to analyse the structure of the crystal. A common method in electron diffraction [15]. The diffraction pattern shows how waves would pass through the crystal. In our simulation, the diffraction pattern is essentially the Fourier transform of the crystal lattices. The diffraction pattern is a powerful way to determine what rotational symmetry the crystal has by counting the dots in the circles. For example, in figure 5, we see a twelve-fold rotational symmetry. This is a symmetry that is not allowed in the usual crystals. If the material has a rotational symmetry that is not allowed by regular crystals, we can conclude that a quasicrystal has formed [15, 16].

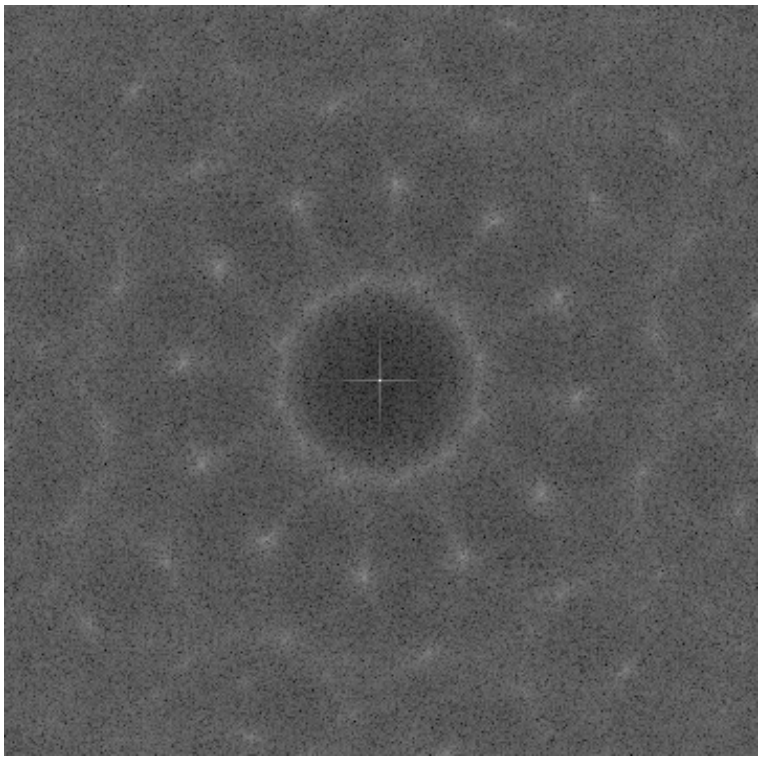

Figure 5: A diffraction pattern obtained from a simulation with parameters $T^* = 0.25, \rho^* = 0.975$, $\delta = 1.4$ after 100 million Monte Carlo cycles. Counting the dots in the circle, it seems this diffraction pattern belongs to a dodecagonal quasicrystal.

3 Results

3.1 Ornstein-Zernike crossover

In this section we use the crossover method as described in section 2.4. The pole analysis is done numerically using the Ornstein-Zernike formula 9. Unfortunately, I was not able to produce a correct pole analysis for the total correlation functions $h(r)$. This might have multiple reasons, which will be discussed in section 4.

3.2 Crossover in the pair correlation function $g(r)$

In this section we use the crossover method as described in section 2.5. First, we look at the shoulder $\delta = 1.4$. For this shoulder it is known that there exists a high density dodecagonal quasicrystal with a density ρ^* of about 0.98 at temperatures below $T^* = 0.4$ [9]. Furthermore, there has been found an 18-fold quasicrystal with a slightly higher shoulder of $\delta = 1.43$. This quasicrystal was found at a lower density of $\rho^* = 0.6239$ and temperature of $T^* = 0.0885$ [2].

3.2.1 High density 12-fold quasicrystal (HD12)

To test if the Monte Carlo simulation works correctly, we attempt to recreate the 12-fold quasicrystal. The simulations are performed with parameters $T^* = 0.25, \rho^* = 0.975$, $\delta = 1.4$.

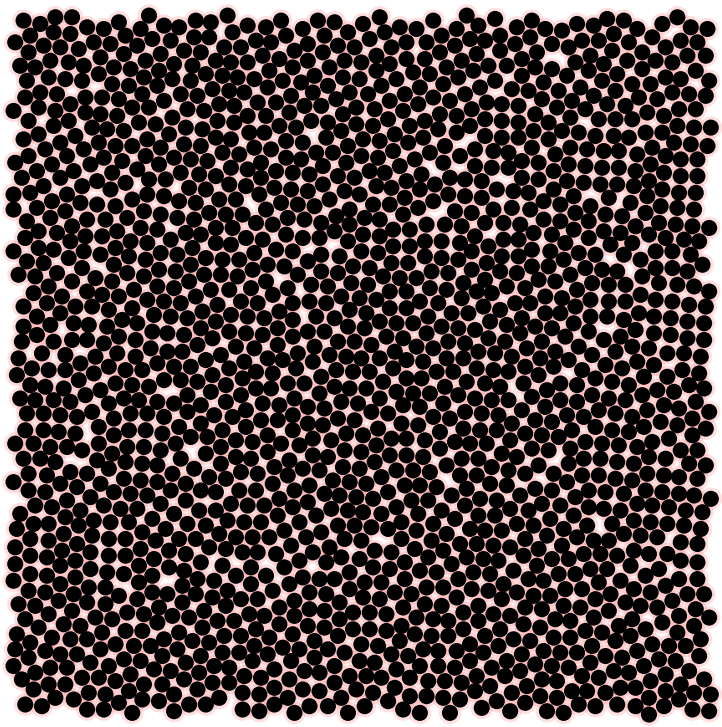

Figure 6: End configuration of system with parameters $T^* = 0.25, \rho^* = 0.975$, $\delta = 1.4$ after 100 million Monte Carlo cycles. There are both square and trigonal structures visible.

The diffraction pattern of figure 6 is shown in figure 5. The diffraction pattern in figure 5 shows a 12-fold rotational symmetry. This confirms the simulation works and a high density dodecagonal quasicrystal does form under these circumstances. In figure 6 we see that both length scales are present (square and trigonal), but it is not a perfect crystal. There are still areas where the crystal is only square, so the quasicrystal is not defect free. These defects might go away if we use more Monte Carlo cycles.

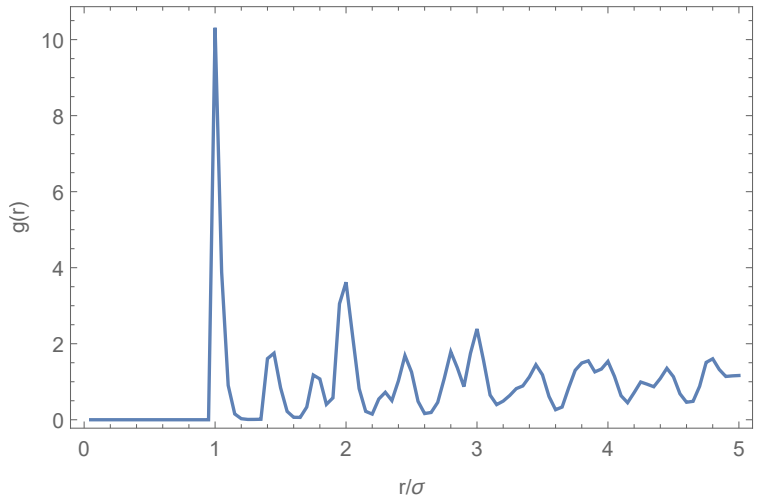

Figure 7: Pair correlation function of simulation with parameters $T^* = 0.25, \rho^* = 0.975$, $\delta = 1.4$. The pair correlation is calculated and averaged over from the last 10 snapshots like figure 6. There is a large peak visible for $r/\sigma = 1$, while the peak at $r/\sigma = 1.4$ is much smaller.

If we look at the pair correlation function in figure 7, it is visible that the peak at $r/\sigma = 1$ or at $r/\sigma = 1.4$ do not have the same height. This way we know this is not the quasicrystal we are looking for, because we expect it to have peaks of the same height.

3.2.2 Low density 18-fold quasicrystal (LD18)

Because the shoulder is close to $\delta = 1.4$, we also take a look at the 18-fold quasicrystal.

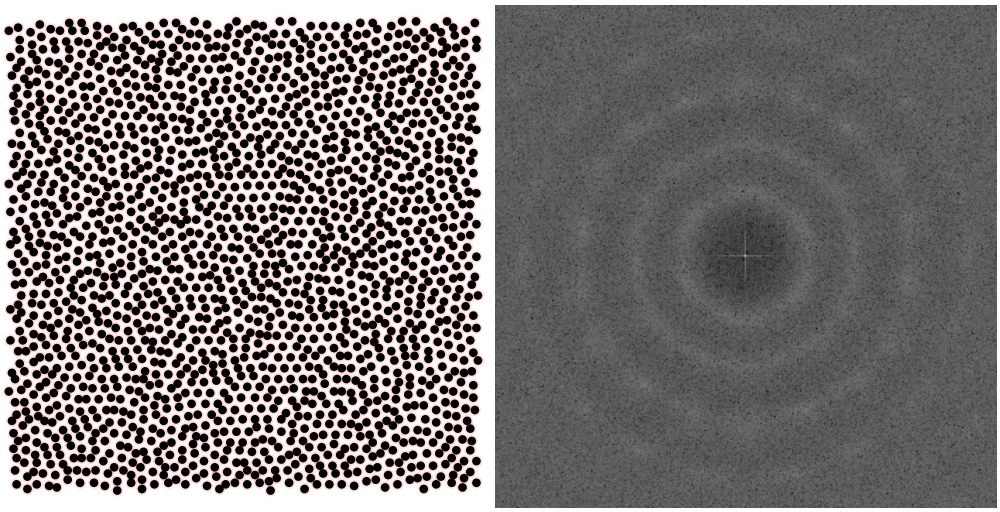

(a) (b)

Figure 8: End configuration (a) and corresponding diffraction pattern (b) of a simulation with parameters $T^* = 0.088, \rho^* = 0.623$, $\delta = 1.43$ after 91 million Monte Carlo steps. We see that an 18-fold rotational symmetry is starting to form.

In figure 8 we see the results of a simulation with parameters $T^* = 0.088, \rho^* = 0.623$ and $\delta = 1.43$ after 91 million Monte Carlo steps. Although the diffraction pattern is not very clear yet, we observe that a crystal with an 18-fold rotational symmetry is starting to form. For the quasicrystal to fully equilibrate it is reported that we need up to 3 billion Monte Carlo steps [2], which is much higher than we were able to achieve.

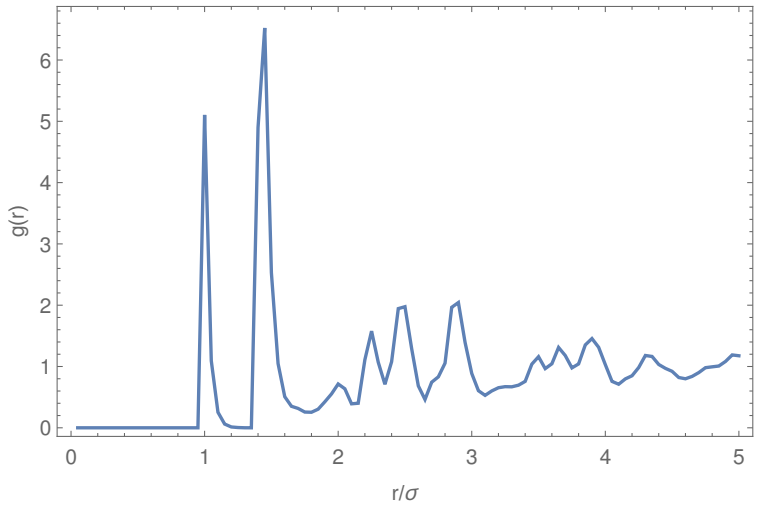

Figure 9: Pair correlation function of system with parameters $T^* = 0.088, \rho^* = 0.623$, $\delta = 1.43$. Both the peak at $r/\sigma = 1$ and $r/\sigma = 1.43$ are present.

In figure 9 we see that the first two peaks of the pair correlation function $g(r)$ are closer to being of equal height than the high density 12 fold quasicrystal. This means that the quasicrystal we are looking for could be related to the 18-fold low density quasicrystal.

To investigate the effect of the shoulder width on the crystal, we also performed a simulation with the same temperature and density, but with shoulder of $\delta = 1.4$.

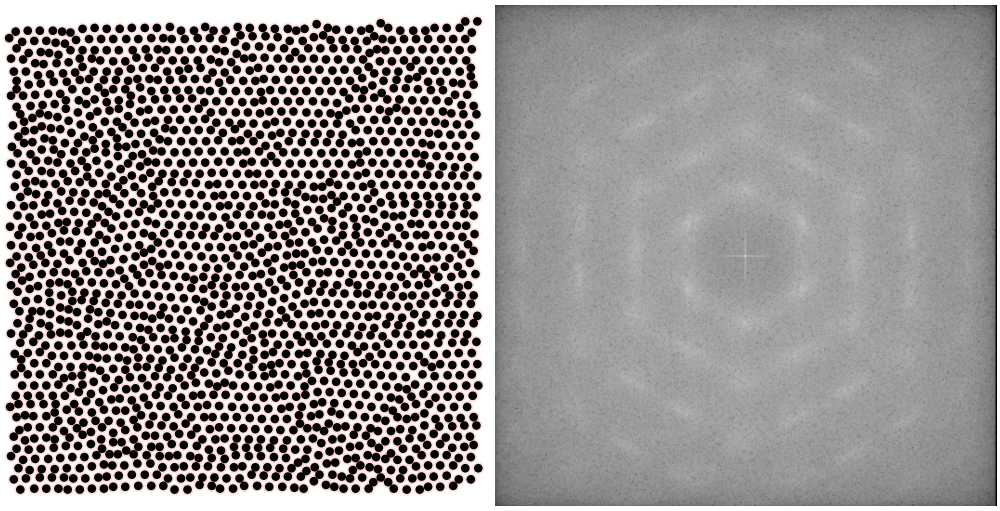

(a) (b)

Figure 10: End configuration (a) and corresponding diffraction pattern (b) of a simulation with parameters $T^* = 0.088, \rho^* = 0.623$, $\delta = 1.4$ after 100 million Monte Carlo steps. The system is in a low density hexagonal state.

In figure 10 we see the end configuration and diffraction pattern of this simulation. We observe that the quasicrystal no longer forms, and that the system ends in a mostly low density hexagonal state.

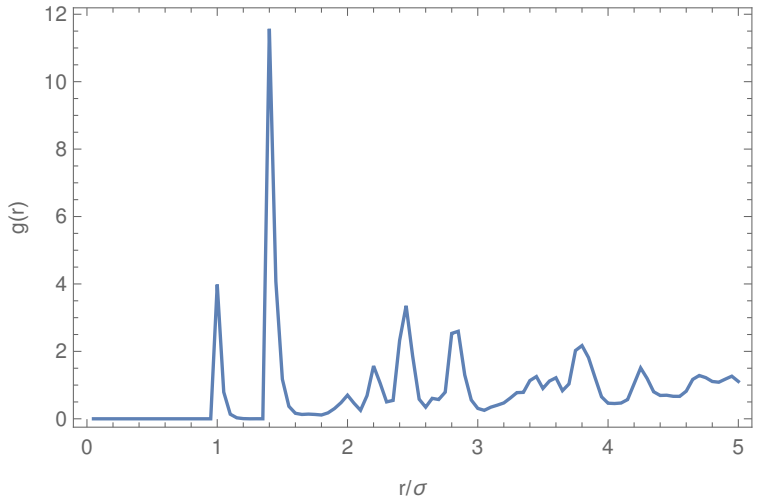

Figure 11: Pair correlation function of system with parameters $T^* = 0.088, \rho^* = 0.623$, $\delta = 1.4$. Both the peak at $r/\sigma = 1$ and $r/\sigma = 1.4$ are present, but the peak of $r/\sigma = 1.4$ is significantly higher.

Looking at the pair correlation function in figure 11, we see that the second peak is quite a bit larger, while the first peak is a bit smaller than the pair correlation function for $\delta = 1.43$. From this, we expect that the crossover of the peaks at $\delta = 1.4$ will occur at a higher density than $\delta = 1.43$.

3.2.3 Crossover line for $\delta = 1.4$

To get an idea of where the crossover at which the peak of $r/\sigma = 1$ becomes bigger than the peak at $r/\sigma = 1.4$, we perform a series of relatively short simulations of 500.000 Monte Carlo cycles. The densities range from $\rho^* = 0.40$ to 0.70 with intervals of 0.01. The temperatures range from $T^* = 0.10$ to 2.0 with intervals of 0.1. The simulations are performed in a box of $N = 418$ particles. The densities and temperatures at which the peaks are of equal height, are determined manually. The result is shown in figure 12. Later, longer and bigger simulations are performed at densities and temperatures near the red line.

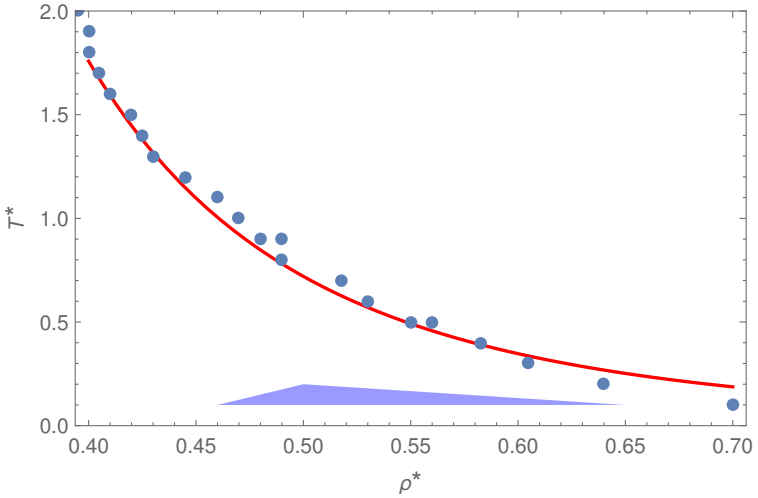

Figure 12: The crossover line. Blue dots represent measured points where the peak of $r/\sigma = 1$ and $r/\sigma = 1.4$ were approximately of equal height. The red line is a fitted curve to these points. The blue triangle approximately marks the area where the simulation is in a solid phase.

In figure 12, the blue dots represent measured points where the peak at $r/\sigma = 1$ and $r/\sigma = 1.4$ are approximately of equal height. The red line in figure 12 is a fitted curve of the form

$$f(x) = \frac{a}{x^b}. \tag{17}$$

In this case $a \approx 0.0469271$ and $b \approx 4$. It is not a perfect fit, especially for the lower temperatures, but it is close enough in our range of densities.

In most points, the simulation is still in fluid phase, except for the measurements with temperatures below $T^* \leq 0.2$. For these temperatures, hexagonal lattices form for densities above $\rho^* \approx 0.46$ and below $\rho^* \approx 0.65$. (These low density hexagonal phases were also measured in the phase diagram of reference [9]). Thus, if quasicrystal formation exists around this line, we expect it to happen only at the very low temperatures. The density is in all cases too low to form a high density dodecagonal quasicrystal, but there might still form an other low density quasicrystal.

A couple of longer simulations are done on and around the red line of figure 12. Some pair correlation functions are shown in figure 13 and corresponding diffraction patterns in figure 14. In figure 13 we see that the peaks at $r/\sigma = 1$ and $r/\sigma = 1.4$ are indeed of the

same height around the red line. This confirms the line of figure 12 is also accurate for longer Monte Carlo simulations with more particles. The diffraction patterns in figure 14 tell us that the simulations are in a fluid phase.

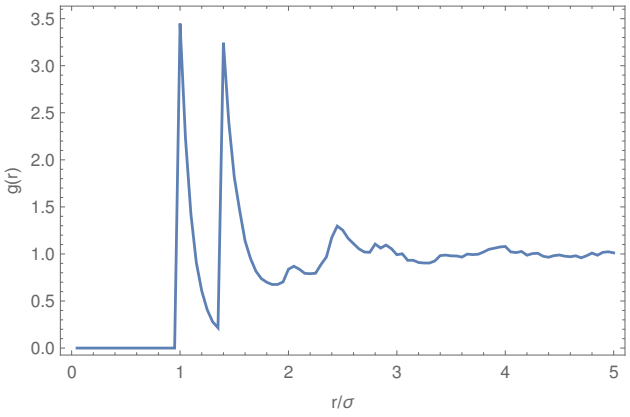

(a) $T^* = 0.230, \rho^* = 0.605, \delta = 1.4$.

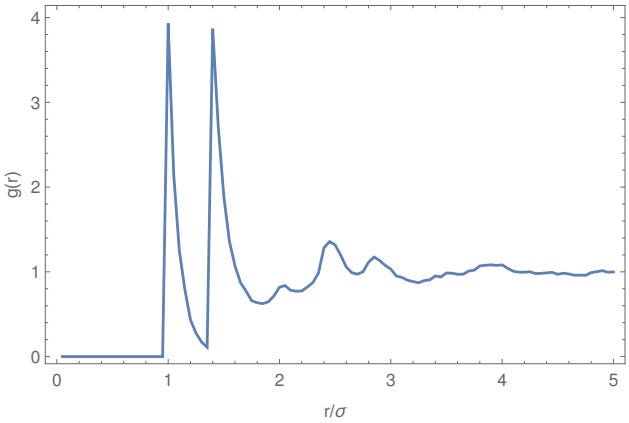

(b) $T^* = 0.250, \rho^* = 0.620, \delta = 1.4$.

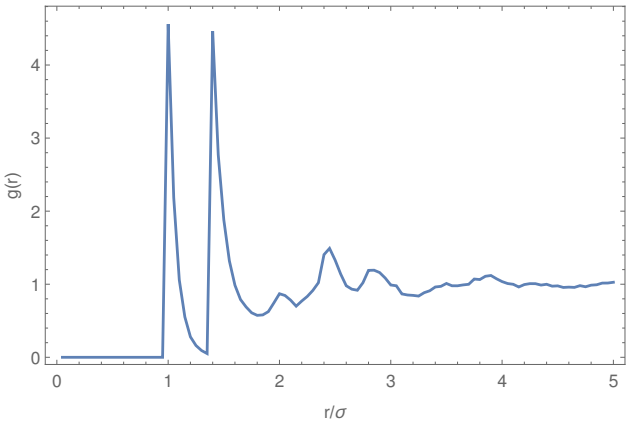

(c) $T^* = 0.200, \rho^* = 0.640, \delta = 1.4$.

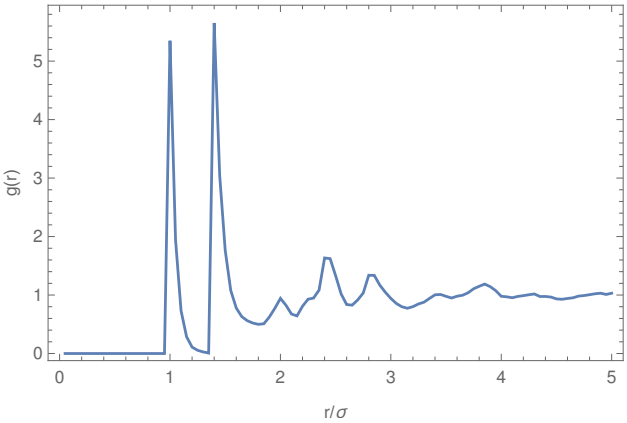

(d) $T^* = 0.250, \rho^* = 0.660, \delta = 1.4$.

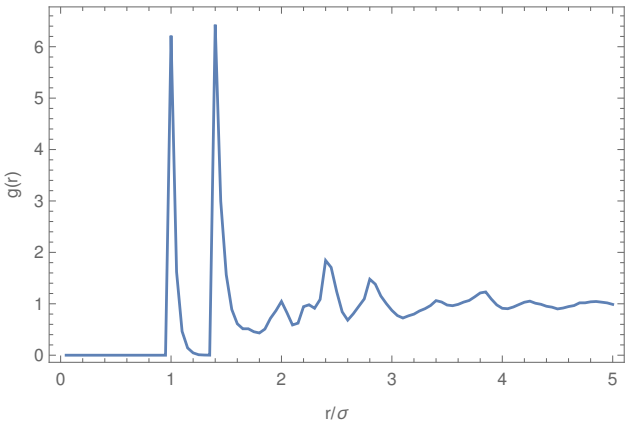

(e) $T^* = 0.111, \rho^* = 0.680, \delta = 1.4$.

Figure 13: Pair correlation functions of various simulations around the red line of figure 12 after 100 million Monte Carlo cycles. It is visible that the peaks at $r/\sigma = 1$ and $r/\sigma = 1.4$ are close to be the same height. Note that y axis differs in the pictures.

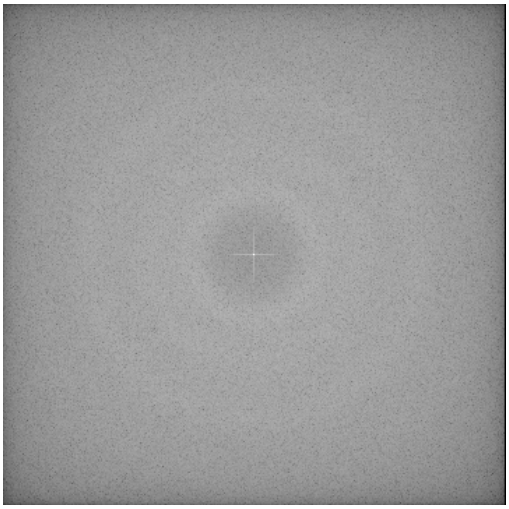

(a) $T^* = 0.230, \rho^* = 0.605$, $\delta = 1.4$.

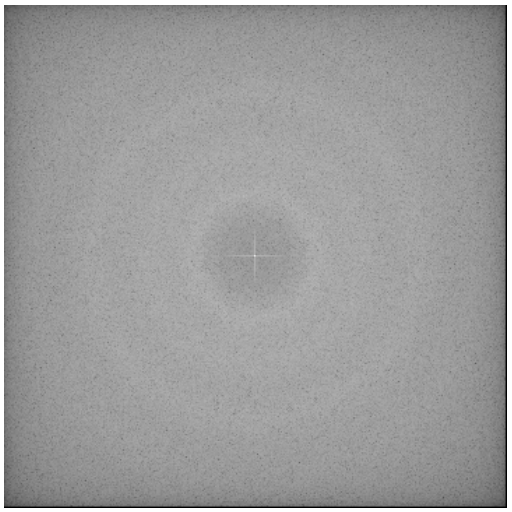

(b) $T^* = 0.250, \rho^* = 0.620$, $\delta = 1.4$.

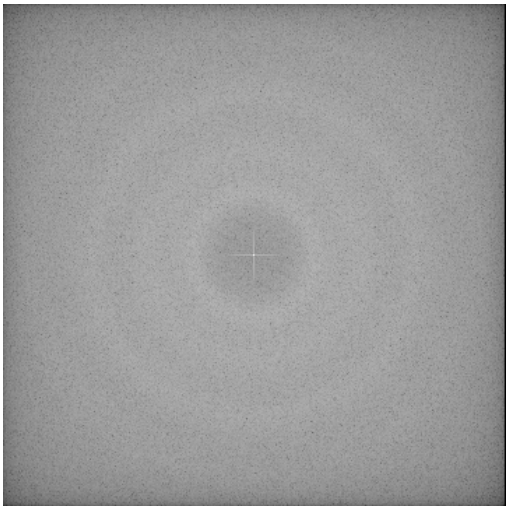

(c) $T^* = 0.200, \rho^* = 0.640$, $\delta = 1.4$.

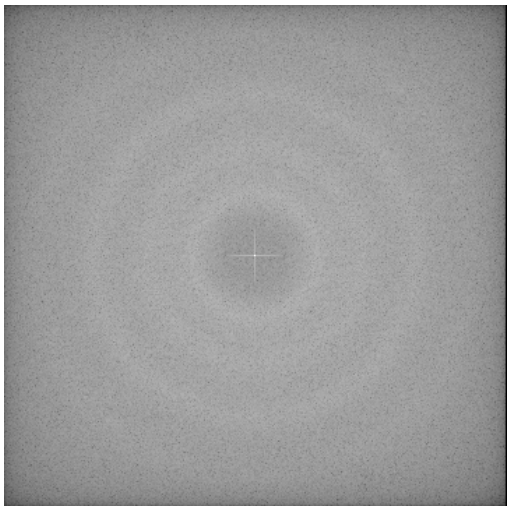

(d) $T^* = 0.250, \rho^* = 0.660$, $\delta = 1.4$.

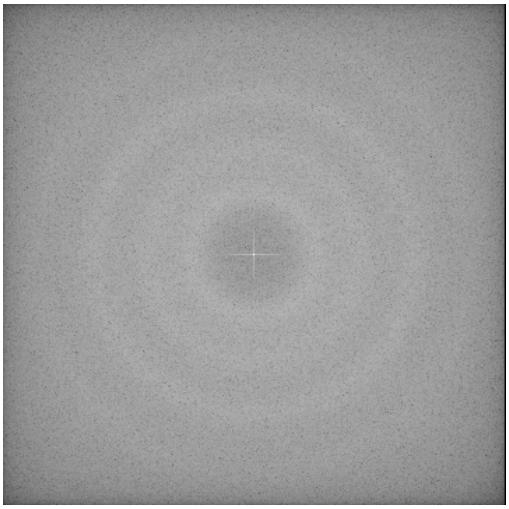

(e) $T^* = 0.111, \rho^* = 0.680$, $\delta = 1.4$.

Figure 14: Diffraction pictures of various simulations around the red line of figure 12 after 100 million Monte Carlo cycles. These pictures show that the simulations are still in a fluid phase.

4 Discussion and conclusion

We have tried to inverse design quasicrystals with single particle Monte Carlo simulations and a square shoulder potential. This was attempted by two different methods. The first method was by finding a crossover in the total correlation function $h(r)$ using the Ornstein-Zernike methods. Unfortunately, with this method, we did not succeed to return any usable results. There are multiple reasons why this method could have failed. Firstly, it is possible that we made a mistake in the derivation of the system of equations used to find the poles q. It is also possible, that the expected forms of $h(r)$ are not a good fit for the square shoulder potential, (especially at distances $r \leq \delta\sigma$). Lastly, we could have made a mistake in the used numerical integration method for the Fourier transforms. We were unable to discover a mistake in one of these potential problems before the end of the project.

The second method was by finding a line in a (T^*, ρ^*) diagram at which the first two peaks in the pair correlation function were of equal height. In a system with shoulder $\delta = 1.4$, we found a line at which we expect quasicrystals to form. If a quasicrystal indeed forms under these circumstances, we expect it to form at low temperatures $T^* < 0.2$. This is because normal crystals at these densities only seem to form at low temperatures. So far, we have not been able to actually find a quasicrystal in this region. As we can see in figure 14, the simulations around this line remain in fluid phase. If we look in figure 12, we see that the line barely touches the area where the simulation is in a solid phase. There have been reports of a low density 18-fold quasicrystal that formed under similar temperature and density, but with a slightly higher shoulder width [2]. Since this low density quasicrystal is not very stable, it is possible that we have not found just the right temperature and density yet for our quasicrystal. It is also possible that the density at which the crossover occurs is just not right for our purpose. In that case we should have chosen a shoulder at which the crossover line clearly crosses a solid phase instead of barely touching it. Finally, the method we use to find quasicrystals could be wrong.

5 Outlook

We could create more plots like figure 12 for different shoulder widths. Possibly, the crossover line goes through a solid phase for an other shoulder. If a situation like this does occur, it would be interesting to investigate if this results in a quasicrystal or not. Doing this could definitively prove if our method of constructing quasicrystals is wrong or not. Another thing we could do is extending our Monte Carlo simulations and use a larger number of particles. Extending the Monte Carlo simulations could help with stabilising the quasicrystals a bit more.

References

[1] D. Levine and P. J. Steinhardt, Phys. Rev. Lett. **53**, 2477 (1984), URL `https://link.aps.org/doi/10.1103/PhysRevLett.53.2477`.

[2] Dotera T, Oshiro T, and Ziherl P, Nature **506**, 208 (2014), ISSN 0028-0836.

[3] D. Shechtman, I. Blech, D. Gratias, and J. W. Cahn, Phys. Rev. Lett. **53**, 1951 (1984), URL https://link.aps.org/doi/10.1103/PhysRevLett.53.1951.

[4] Bindi L, Steinhardt PJ, Yao N, and Lu PJ, Science (New York, N.Y.) **324**, 1306 (2009), ISSN 0036-8075.

[5] P. W. Leung, C. L. Henley, and G. V. Chester, Phys. Rev. B **39**, 446 (1989), URL https://link.aps.org/doi/10.1103/PhysRevB.39.446.

[6] H. G. Schoberth, H. Emmerich, M. Holzinger, M. Dulle, S. Frster, and T. Gruhn, Soft Matter **12**, 7644 (2016), URL http://dx.doi.org/10.1039/C6SM01454B.

[7] H. Pattabhiraman and M. Dijkstra, The Journal of Chemical Physics **146**, 114901 (2017), https://doi.org/10.1063/1.4977934, URL https://doi.org/10.1063/1.4977934.

[8] D. A. Young and B. J. Alder, Phys. Rev. Lett. Physical Review Letters **38**, 1213 (1977), ISSN 0031-9007.

[9] Pattabhiraman H, Gantapara AP, and Dijkstra M, The Journal of chemical physics **143** (2015), ISSN 0021-9606.

[10] H. Pattabhiraman and M. Dijkstra, J. Phys.: Condens. Matter Journal of Physics: Condensed Matter **29**, 094003 (2017), ISSN 0953-8984.

[11] D. A. Young and B. J. Alder, Phys. Rev. Lett. **38**, 1213 (1977), URL https://link.aps.org/doi/10.1103/PhysRevLett.38.1213.

[12] M. Dijkstra, *Modelling and Simulation* (2018).

[13] M. C. Walters, P. Subramanian, A. J. Archer, and R. Evans, Phys. Rev. E Physical Review E **98** (2018), ISSN 2470-0045.

[14] M. Dijkstra and R. Evans, The Journal of Chemical Physics **112**, 1449 (2000), https://doi.org/10.1063/1.480598, URL https://doi.org/10.1063/1.480598.

[15] Z. M. Stadnik, M. Cardona, P. Fulde, K. von Klitzing, R. Merlin, H.-J. Queisser, and H. Strmer, eds., *Physical Properties of Quasicrystals*, vol. 126 of *Springer Series in Solid-State Sciences* (Springer Berlin Heidelberg, Berlin, Heidelberg, 1999), ISBN 978-3-642-63593-9 978-3-642-58434-3, URL http://link.springer.com/10.1007/978-3-642-58434-3.

[16] D. V. Talapin, E. V. Shevchenko, M. I. Bodnarchuk, X. Ye, J. Chen, and C. B. Murray, Nature **461**, 964 (2009), URL https://doi.org/10.1038/nature08439.